

Intersubband gain in a Bloch oscillator and Quantum cascade laser

H. Willenberg,^{1,2,*} G.H. Döhler,² and J. Faist¹

¹*Institut de Physique, Université de Neuchâtel, Switzerland*

²*Institut für technische Physik, Universität Erlangen, Germany*

(Dated: October 25, 2018)

The link between the inversion gain of quantum cascade structures and the Bloch gain in periodic superlattices is presented. The proposed theoretical model based on the density matrix formalism is able to treat the gain mechanism of the Bloch oscillator and Quantum cascade laser on the same footing by taking into account in-plane momentum relaxation. The model predicts a dispersive contribution in addition to the (usual) population-inversion-dependent intersubband gain in quantum cascade structures and – in the absence of inversion – provides the quantum mechanical description for the dispersive gain in superlattices. It corroborates the predictions of the semi-classical miniband picture, according to which gain is predicted for photon energies lower than the Bloch oscillation frequency, whereas net absorption is expected at higher photon energies, as a description which is valid in the high-temperature limit. A red-shift of the amplified emission with respect to the resonant transition energy results from the dispersive gain contribution in any intersubband transition, for which the population inversion is small.

I. INTRODUCTION

Soon after the original proposal of semiconductor superlattices¹, two apparently quite different schemes to obtain optical gain in such novel systems were put forward. In a seminal work, Kazarinov and Suris pointed out how to achieve a population inversion, a key ingredient to obtain light amplification, between electronic subbands in a strongly biased superlattice². On the other hand, based on semi-classical arguments, Ktitorov *et al.*³ and later Ignatov *et al.*⁴ predicted optical gain due to Bloch oscillations within a miniband – despite a missing population inversion.

Two decades later, the demonstration of the quantum cascade laser⁵ affirmed the first proposal. The (conduction) band structure in each period is carefully designed to allow for injecting electrons into an upper subband state, with a long non-radiative lifetime, and to enable a fast extraction of electrons from an accordingly tailored lower state. As a consequence, population inversion is achieved. Also, by a suitable design, the structure is electrically stable at threshold. By now, the quantum cascade laser technology covers a wide range of the electro-magnetic spectrum. Recently, a room-temperature continuous-wave laser⁶ emitting at a wavelength of $9\mu\text{m}$ has been demonstrated and stimulated emission in the terahertz regime at about $66\mu\text{m}$ ^{7,8} has been observed.

In contrast to this, the feasibility of the Bloch oscillator, emitting electro-magnetic radiation, tunable by the external electric dc field, is still under question. Besides the task to stabilize the electric field domains in a biased superlattice at the point of operation, the description of the gain mechanism is, so far, based on semi-classical models only. In a naive picture, electro-magnetic radiation of photon energy $\hbar\omega \approx \hbar\omega_b = eFd$ is expected, corresponding to the frequency of Bloch oscillations ω_b that linearly depends on the applied dc field F . For, *e.g.* a superlattice period d of some nanometers and fields of

several tenth of kV/cm, the photon frequencies are in the terahertz range.

In fact, semi-classical calculations exhibit neither gain nor absorption at resonance, *i.e.* for $\omega = \omega_b$, but transparency. Particularly in the quantum-mechanical picture, it is evident that only spontaneous transitions can occur at resonance. At sufficiently high electric fields, the miniband is split into the Wannier-Stark ladder, a set of states evenly spaced by eFd in energy. Resonant stimulated emission processes between adjacent states are balanced by absorption processes, because of the translational symmetry of the system, which dictates equal occupation for all rungs of the Wannier-Stark ladder.

Nevertheless, the semi-classical calculation does predict gain – without inversion – for non-resonant transitions with a "too small" photon energy, $\hbar\omega < \hbar\omega_b$, and absorption for $\hbar\omega > \hbar\omega_b$. But the existence and strength of this semi-classically predicted Bloch gain is still discussed, despite experimental observation of many related phenomena in superlattices, such as negative differential conductivity⁹, the associated Bloch oscillations¹⁰ and the coupling of the superlattice to external THz radiation^{11,12}, just to mention a few. In particular, the gain mechanism is lacking an interpretation in terms of the quantum-mechanical Wannier-Stark picture.

In this paper such a quantum-mechanical interpretation of the Bloch gain in superlattices is suggested and a link is established between the intersubband gain originating from a population inversion, with its symmetric spectral shape centered at the transition energy, and the dispersive gain predicted for a periodic superlattice, with its nearly anti-symmetric profile. The quantum-mechanical model, based on the density matrix formalism similar to the one employed earlier¹³, yields a general expression for the gain profile in intersubband transitions.

In Sec. II we present the model system, and discuss assumptions and details of the density matrix calculation. With less stringent approximations than those made by Kazarinov and Suris we find an expression for the coher-

ence between two, at first spatially separated, subband states that are coupled by tunneling and broadened by intra-subband scattering. The coherence determines current density as well as optical transitions. Transforming to the basis of eigenstates of the biased heterostructure – the Wannier-Stark basis for the superlattice – the model is extended to describe optical transitions between any pair of subbands.

In Sec. III we apply the theory to superlattices and obtain the quantum mechanical counterparts to the semi-classical results for both the Esaki-Tsu current-voltage characteristics and the dispersive Bloch gain. The results are quantitatively compared to the predictions of the semi-classical picture, where good agreement is found for higher electron temperatures.

In Sec. IV intersubband transitions are investigated for the quantum cascade structure and the relation between (anti-symmetric) Bloch gain and Lorentzian-shaped intersubband gain becomes apparent: the theory predicts a transition from the Lorentzian shaped inversion gain to the dispersive Bloch gain with decreasing population inversion accompanied by a red-shift of the peak gain with respect to the transition energy.

II. THEORY

We consider two subbands, confined in adjacent wells, that serve as a model system for photon-assisted tunneling structures and, in particular, for transitions within the Wannier-Stark ladder of a weakly coupled superlattice. To start with, the same basis as in the original work of Kazarinov and Suris is chosen as an appropriate basis set. The wave functions $|ik\rangle$ are given by the product of the envelope functions $\Psi_i(z)$, maximally localized¹⁴ in well i , and plane waves

$$\langle \mathbf{r}, z | ik \rangle = \Psi_i(z) e^{i\mathbf{k}\cdot\mathbf{r}}, \quad (1)$$

where the z -axis is defined by the direction of growth, $\mathbf{k} = (k_x, k_y) \equiv k$ denotes the in-plane momentum and $\mathbf{r} = (x, y)$ the lateral position. The matrix elements of the Hamiltonian in this basis are given by

$$\mathcal{H}_{kk'}^{ij} = \langle ik | \mathcal{H} | jk' \rangle = H_{kk'}^{ij} \delta_{kk'} + V_{kk'}^{ij}, \quad (2)$$

where the respective contributions H and V take the form

$$H_k^{ij} = \begin{pmatrix} \epsilon_{2k} & \hbar\Omega_{21} \\ \hbar\Omega_{12} & \epsilon_{1k} \end{pmatrix}^{ij}, \quad V_{kk'}^{ij} = \begin{pmatrix} V_{kk'}^{22} & 0 \\ 0 & V_{kk'}^{11} \end{pmatrix}^{ij}. \quad (3)$$

Thus, electrons are allowed to tunnel between the subband state i and j by means of the momentum conserving matrix elements $\hbar\Omega_{ij}$, in each of which they are possibly scattered out of a virtual intermediate state by an intra-well relaxation process $V_{kk'}^{ii}$, as depicted in Fig. 1. For simplicity we restrict ourselves to elastic (impurity, *e.g.*) scattering within each subband and assume a parabolic

dispersion relation parallel to the layers in the effective mass approximation

$$\epsilon_{ik} = \epsilon_i + \frac{\hbar^2 k^2}{2m^*}, \quad (4)$$

where ϵ_i denotes the lower subband edge and m^* is the effective mass of the electron averaged over the extension of the wave function in well and barrier.

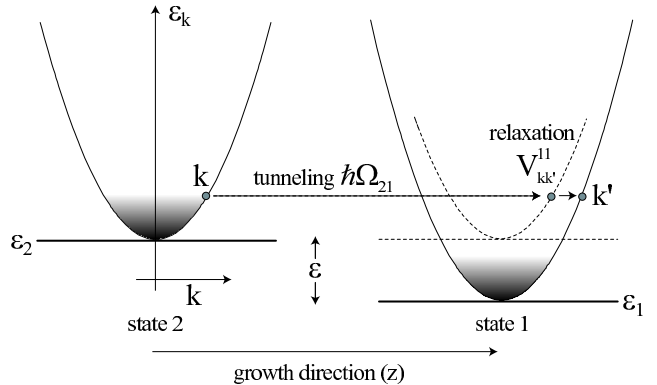


FIG. 1: Mixed momentum and real-space picture of a two-level-system that serves as a simple model for a diagonal intersubband transition. Tunneling into a virtual intermediate state (dotted) as well as photon-assisted tunneling is expressed by a transfer matrix element $\hbar\Omega_{ij}$. Relaxation is assumed to take place within each subband only.

A. Coherences

Using the equation of motion of the density matrix $i\hbar \partial_t \hat{\rho} = [\mathcal{H}, \hat{\rho}]$ and separating the diagonal and non-diagonal part with respect to the parallel momentum k, k' according to $\hat{\rho}_{kk'}^{ij} = \delta_{kk'} \rho_k^{ij} + (1 - \delta_{kk'}) \rho_{kk'}^{ij}$, we obtain two coupled equations with four terms each, which determine the time evolution of the system. Since the coherent term H is diagonal with respect to the in-plane momentum and the scattering term V is purely non-diagonal, the commutators that determine the diagonal and non-diagonal part of the density matrix are evaluated as

$$i\hbar \partial_t \rho_k^{ij} = \sum_m (H_k^{im} \rho_k^{mj} - \rho_k^{im} H_k^{mj}) + \sum_{m,k'} (V_{kk'}^{im} \rho_{k'}^{mj} - \rho_{kk'}^{im} V_{k'k}^{mj}) \quad (5)$$

$$i\hbar \partial_t \rho_{kk'}^{ij} \approx \sum_m (V_{kk'}^{im} \rho_{k'}^{mj} - \rho_{kk'}^{im} V_{kk'}^{mj}) + \sum_m (H_k^{im} \rho_{kk'}^{mj} - \rho_{kk'}^{im} H_{k'}^{mj}), \quad (6)$$

where the commutator of the scattering potential with the non-diagonal part of ρ has been neglected in the second equation (Born approximation). The steady-state values of the coherences of the density matrix f^{ij} , which

determine the transitions $|ik\rangle \rightarrow |jk\rangle$, the current and the absorption, are obtained from a Laplace average¹⁵ defined by

$$f(s) = s \int_0^\infty dt e^{-st} \rho(t) \quad (7)$$

and performing the Laplace limit $s \rightarrow 0$ using the relation $\lim_{s \rightarrow 0^+} (\omega - is)^{-1} = P(1/\omega) + i\pi\delta(\omega)$ at the appropriate stage of the calculation. In this approach the populations f_k^{ii} of the density matrix are not accessible and appear in the resulting expression as external quantities. The Laplace average gives

$$\begin{aligned} i\hbar s f_k^{ij} &= i\hbar s \rho_k^{ij}(0) + \sum_m (H_k^{im} f_k^{mj} - f_k^{im} H_k^{mj}) \\ &+ \sum_{m,k'} (V_{kk'}^{im} f_{k'k}^{mj} - f_{kk'}^{im} V_{k'k}^{mj}) \end{aligned} \quad (8)$$

$$\begin{aligned} i\hbar s f_{kk'}^{ij} &\approx i\hbar s \rho_{kk'}^{ij}(0) + \sum_m (V_{kk'}^{im} f_{k'k}^{mj} - f_{kk'}^{im} V_{k'k}^{mj}) \\ &+ \sum_m (H_k^{im} f_{kk'}^{mj} - f_{kk'}^{im} H_{k'}^{mj}). \end{aligned} \quad (9)$$

In a first step, the non-diagonal part in equation (9) is approximated (*cf.* appendix A for details). Specifying to the assumptions of a two-level-system with intra-well scattering only and neglecting terms of higher order in Ω_{ij} corresponding to multiple tunneling processes, gives

$$\begin{aligned} (f)_{kk'}^{ij} &\approx i\pi\delta(\epsilon_{ik} - \epsilon_{jk'}) (V_{kk'}^{ii} f_{k'}^{ij} - f_{kk'}^{ij} V_{kk'}^{jj} + \\ &+ \hbar\Omega_{ij} \left(\frac{V_{kk'}^{jj} (f_{jk}^{jj} - f_{k'}^{jj})}{\epsilon_{jk} - \epsilon_{jk'}} - \frac{V_{kk'}^{ii} (f_k^{ii} - f_{k'}^{ii})}{\epsilon_{ik} - \epsilon_{ik'}} \right), \end{aligned} \quad (10)$$

which has to be placed into equation (8) for the diagonal part. Simplifying for intra-well scattering here and taking the Laplace limit yields (*cf.* appendix B)

$$\begin{aligned} (\epsilon_{ik} - \epsilon_{jk}) f_k^{ij} &= \hbar\Omega_{ij} (f_k^{ii} - f_k^{jj}) \\ &- \sum_{k'} (V_{kk'}^{ii} (f)_{k'k}^{ij} - (f)_{kk'}^{ij} V_{k'k}^{jj}), \end{aligned} \quad (11)$$

where (f) denotes the approximated expression for the non-diagonal part in equation (10). Performing an ensemble average, *i.e.* dropping terms related to correlation effects in the scattering potential, we obtain

$$\begin{aligned} &(\epsilon_{ik} - \epsilon_{jk}) f_k^{ij} - i\pi f_k^{ij} \times \\ &\times \sum_{k'} \delta(\epsilon_{ik'} - \epsilon_{jk}) |V_{kk'}^{ii}|^2 + \delta(\epsilon_{ik} - \epsilon_{jk'}) |V_{kk'}^{jj}|^2 \\ &= \hbar\Omega_{ij} (f_k^{ii} - f_k^{jj}) + \\ &+ i\pi \sum_{k'} [\delta(\epsilon_{ik'} - \epsilon_{jk}) |V_{kk'}^{ii}|^2 \frac{\hbar\Omega_{ij}}{\epsilon_{ik'} - \epsilon_{ik}} (f_{k'}^{ii} - f_k^{ii}) \\ &+ \delta(\epsilon_{ik} - \epsilon_{jk'}) |V_{kk'}^{jj}|^2 \frac{\hbar\Omega_{ij}}{\epsilon_{jk} - \epsilon_{jk'}} (f_k^{jj} - f_{k'}^{jj})], \end{aligned} \quad (12)$$

which agrees with the previous result¹³. In contrast to the original treatment, we continue by neither neglecting the difference of the arguments in the δ -functions on

the LHS nor omitting the second term on the RHS. The coherence associated with the transition $|2k\rangle \rightarrow |1k\rangle$ is obtained from

$$\begin{aligned} \epsilon f_k^{21} - \overbrace{i(\gamma_k^2 + \gamma_k^1)}^{\text{transition broadening}} f_k^{21} &= \overbrace{\hbar\Omega_{21} (f_k^{22} - f_k^{11})}^{\text{population difference}} \\ &+ \underbrace{i\hbar\Omega_{21} \epsilon^{-1} (\gamma_k^2 (f_{q-}^{22} - f_k^{22}) - \gamma_k^1 (f_{q+}^{11} - f_k^{11}))}_{\text{Bloch type contribution}}, \end{aligned} \quad (13)$$

where we have used abbreviations for the scattering induced broadening of the transition $\gamma_k^i = \sum_{k'} \delta(\epsilon_{ik'} - \epsilon_{jk}) |V_{kk'}^{ii}|^2$, the subband separation $\epsilon = \epsilon_{2k} - \epsilon_{1k}$ and the in-plane momentum of the final state $q_\pm = \hbar^{-1} \sqrt{2m^*(\epsilon_k \pm \epsilon)}$. The first term on the RHS, which contains the difference of populations between the two states, corresponds to the central result of Reference¹³, cited often as the original proposal of the quantum cascade laser. The second term, which has been discarded so far, contains differences in population within a subband. It is this term which will be responsible for the second order type of gain, leading to the characteristic negative differential conductivity and the dispersive gain profile in a superlattice, and a modified spectral shape of the gain in a quantum cascade laser.

B. Current density

The current density between two states spatially separated by $d = z_{22} - z_{11}$ is calculated from $j = e \text{Tr}(\hat{v}f)$, where $\hat{v} = i/\hbar[H, z]$ is the velocity operator and z is the position operator. The current is induced by the non-diagonal matrix elements of the velocity operator v_{ij} , which are given by $v_{ij} = i\Omega_{ij}(z_{jj} - z_{ii}) + \epsilon z_{ij}/\hbar$. By choice of the basis set, the contribution of the dipole z_{ij} is small compared to the tunneling term¹³ and we obtain

$$j \approx ed \sum_k i(\Omega_{21} f_k^{12} - \Omega_{12} f_k^{21}). \quad (14)$$

Using the previous equation for the coherences f_k^{12} and f_k^{21} and the current yields

$$j = \frac{ed|\hbar\Omega_{21}|^2}{\hbar} \sum_k \frac{\gamma_k^1 (f_k^{22} - f_{q+}^{11}) + \gamma_k^2 (f_{q-}^{22} - f_k^{11})}{\epsilon^2 + (\gamma_k^1 + \gamma_k^2)^2}. \quad (15)$$

The current results from differences in population. In the following section, and in contrast to the original work, the differences are evaluated for non-equivalent k -states in the respective subbands. To obtain the result of Kazari-nov and Suris, q_\pm is set equal to k and a constant broadening γ is used

$$j \approx \frac{ed|\hbar\Omega_{21}|^2}{\hbar} \frac{\gamma}{\epsilon^2 + \gamma^2} \Delta n.$$

With this approximation, the current density is solely driven by the density of excess electrons in either state

$\Delta n = \sum_k (f_k^{22} - f_k^{11})$. For a superlattice, this approximation does predict the resonant current peaks that occur whenever ground and excited states align, but fails to account for the current between equivalent states in the Wannier-Stark ladder.

C. Absorption and gain

Optical properties are deduced from the high-frequency response to an additionally applied ac field. In the case of a photon-assisted tunneling transition, the Hamiltonian is supplemented by

$$\delta H(t) = -\frac{e}{c} \hat{v} A = \begin{pmatrix} 0 & \frac{edf_\omega}{\omega} \Omega_{21} e^{-i\omega t} \\ \frac{edf_\omega}{\omega} \Omega_{12} e^{i\omega t} & 0 \end{pmatrix} \quad (16)$$

for a vector potential $A = (c/i\omega) f_\omega e^{-i\omega t}$ with an amplitude f_ω of the high-frequency field. Noting the similar structure of δH and the non-diagonal part of H , the corrections to the coherences in linear response δf_k^{21} and δf_k^{12} are related to f_k^{21} and f_k^{12} by

$$\delta f_{k,\omega}^{21} = -\frac{edf_\omega}{\hbar\omega} f_{k,\epsilon-\hbar\omega}^{21} \quad \text{and} \quad \delta f_{k,\omega}^{12} = \frac{edf_\omega}{\hbar\omega} f_{k,\epsilon+\hbar\omega}^{12}, \quad (17)$$

which are evaluated at an energy $\epsilon \pm \hbar\omega$ instead of ϵ due to the time dependence of the ac field. This relation reflects the similarity of tunneling and photon-assisted tunneling processes in a diagonal transition. The photon-induced current becomes

$$\delta j(\omega) \approx ed \sum_k i(\Omega_{21} \delta f_{k,\omega}^{12} - \Omega_{12} \delta f_{k,\omega}^{21}). \quad (18)$$

The high-frequency conductivity is related to the current by $\sigma(\omega) = \partial(j + \delta j(\omega))/\partial f_\omega$, and directly linked to the absorption (*cf.* appendix C for details) according to

$$\alpha(\omega) = \frac{\Re(\sigma(\omega))}{\varepsilon_0 n_r c} = -\frac{e^2 d^2 |\Omega_{21}|^2}{\varepsilon_0 n_r c \omega} \times \sum_k \frac{\gamma_k^1 (f_k^{22} - f_{k_+}^{11}) + \gamma_k^2 (f_{k_-}^{22} - f_k^{11})}{(\epsilon - \hbar\omega)^2 + (\hbar\tau_k^{-1})^2}. \quad (19)$$

The in-plane momenta of the final states are denoted by $k_\pm = \hbar^{-1} \sqrt{2m^*(\epsilon_k \pm (\epsilon - \hbar\omega))}$. The preceding expression contains the two gain mechanisms as limiting cases of a more general intersubband gain profile with a simple physical interpretation. Before we discuss the quantum-mechanical paths involved, the expression may be generalized to an arbitrarily located pair of subband states.

To account for vertical as well as diagonal transitions the basis of eigenstates of the biased system – the Wannier-Stark basis for a superlattice – is chosen. Due to the assumption of intra-well scattering only, the dark current vanishes as the tunneling matrix element $\hbar\Omega_{ij}$ is incorporated in the extended wave functions. The photon-induced current, however, is then mediated by the dipole

matrix element between the two subband states, which can no longer be considered as small in this basis. The non-diagonal part of the velocity operator is given by $v_{ij} = i\epsilon z_{ij}$. Since the operator of the high frequency field $\delta H = -e/c\hat{v}A$ does not change its purely non-diagonal structure, inspection of the previous equations and replacement of $i d\Omega_{ij}$ by $i\epsilon z_{ij}/\hbar$ naturally extends the equation for the gain profile to any intersubband transition and permits to omit the rather arbitrary distinction between a diagonal and vertical transition

$$\alpha(\omega) = -\frac{e^2 |z_{21}|^2 \epsilon^2}{\varepsilon_0 n_r c \hbar^2 \omega} \sum_k \frac{\gamma_k^1 (f_k^{22} - f_{k_+}^{11}) + \gamma_k^2 (f_{k_-}^{22} - f_k^{11})}{(\epsilon - \hbar\omega)^2 + (\gamma_k^1 + \gamma_k^2)^2}. \quad (20)$$

As will be shown in the following, expression (20) allows a simple explanation of the gain mechanism in a superlattice and in a quantum cascade structure. It is instructive to rewrite the differences in populations as

$$\gamma_k^1 (f_k^{22} - f_{k_+}^{11}) = \underbrace{\gamma_k^1 (f_k^{22} (1 - f_{k_+}^{11}) - f_{k_+}^{11} (1 - f_k^{22}))}_{\text{emission } |2\rangle \rightarrow |1\rangle}, \quad (21)$$

which directly translate into the paths depicted in Fig. 2. The two processes above relate the states $|2k\rangle$ and $|1k_+\rangle$ by the emission or absorption of a (non-resonant) photon, $\hbar\omega \neq \epsilon$ for $k \neq k_+$, assisted by relaxation within the lower state via $\gamma_{k_+}^1$, which ensures momentum transfer. The second difference in equation (20) is interpreted accordingly, where the relaxation takes place within the upper state.

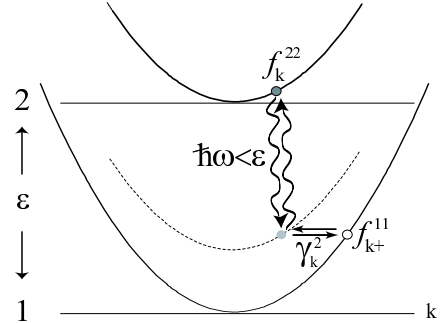


FIG. 2: Possible quantum-mechanical paths: for an incident photon with energy $\hbar\omega \neq \epsilon$, absorption or stimulated emission may occur due to a non-resonant absorption or emission into an intermediate and a subsequent relaxation into the final state. Energy and momentum are conserved in this second order process.

If one assumes constant and equal in-plane scattering times $\tau = \hbar/\gamma$, a Fermi distribution with the same temperature T in each subband and chemical potentials μ_1 and μ_2 , respectively, the gain is analytically expressed as

$$\alpha(\omega) = \frac{e^2 |z_{12}|^2 \epsilon^2}{\varepsilon_0 n_r c \hbar^2 \omega} \frac{m^* k_b T}{\pi \hbar^2} \frac{\gamma}{\delta^2 + \gamma^2} \times \ln \left(\frac{e^{(\mu_1 - \epsilon_1)/k_b T} e^{-\delta/k_b T} + \hat{\theta}(\delta)}{e^{(\mu_2 - \epsilon_2)/k_b T} + \hat{\theta}(\delta)} \right), \quad (22)$$

where $\delta = \epsilon - \hbar\omega$ characterizes the off-resonant nature of the photon transition and $\hat{\theta}(\delta) = \theta(\delta) + \theta(-\delta)e^{-\delta/k_bT}$ reflects the asymmetry between "too small" and "too large" photons with regard to the resonant transition.

III. RESULTS

In this part the theoretical model is evaluated and interpreted with respect to the gain profile of a superlattice and quantum cascade laser.

A. Bloch oscillator

In the case of a superlattice, populations and scattering times are equal for symmetry reasons, $f_k^{11} = f_k^{22}$ and $\gamma_k^1 = \gamma_k^2$. The characteristic negative differential conductivity of the current-voltage characteristic $j(F)$ is recovered from equation (15) if one identifies the subband spacing with the field drop per period, $\epsilon = eFd$, where F is the applied electric field. The current density reads

$$j(F) = \frac{ed\Delta^2}{4\hbar} \sum_k \frac{\gamma_k(f_{k-} - f_{k+})}{(eFd)^2 + (2\gamma_k)^2}, \quad (23)$$

where we omitted the state indices and introduced the miniband width via $\Delta \approx 4\hbar\Omega_{12}$. The populations may be described by thermal distributions, either by Fermi-Dirac or Boltzmann statistics. The current-voltage characteristic resembles the Esaki-Tsu characteristic and agrees quantitatively with the result by Wacker *et al.*¹⁶ within the sequential tunneling picture¹⁷ valid for weakly coupled superlattices. This assumption is implicit in the present approach, as we allow only for next-neighbor interaction and multiple tunneling is excluded, corresponding to a limited coherence of spatially extended states.

Rewriting the gain profile of equation (20) specifically for a superlattice yields

$$\alpha(\omega) = -\frac{e^2 d^2 |\frac{1}{4}\Delta|^2}{\epsilon_0 n_r c \hbar^2 \omega} \sum_k \frac{\gamma_k(f_{k-} - f_{k+})}{(eFd - \hbar\omega)^2 + (2\gamma_k)^2}, \quad (24)$$

Note, as the miniband width of a superlattice, Δ , and the dipole matrix element, z_{ij} , are related by¹⁸ $z_{ij} = d\Delta/4eFd$ in the Wannier-Stark basis, the diagonal expression of equation (19) and the general expression of equation (20) for $\alpha(\omega)$ provide identical results. At resonance, the incoming photon provokes transitions between equivalent states, $k_{\pm} = k$, and absorption and emission balance each other as expected from a system with no population inversion, $\Delta n = \sum_k (f_k^{22} - f_k^{11}) = 0$. In the case of photons with energy $\hbar\omega < \epsilon$ the lower state involved in this second order transitions will be less occupied than the upper state, leading to an asymmetry between emission and absorption in favor of gain. In contrast, for a photon energy exceeding the subband spacing absorption occurs. As illustrated in Fig. 3 equation (24)

recovers the dispersive shape of the Bloch gain – giving rise to absorption above and (stimulated) emission below the field-dependent Bloch frequency $\omega_b = eFd/\hbar$. Note, we have neglected any particularity of the actual scattering processes here. A detailed investigation in the framework of second order perturbation theory¹⁹ reveals a complex interplay of population effects and the influence of the momentum transfer for the relaxation processes in a superlattice.

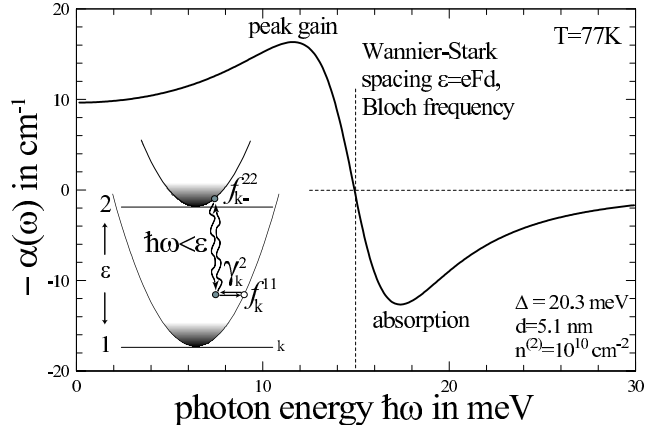


FIG. 3: Bloch oscillator at $\epsilon = eFd = 15\text{meV}$: a dispersive gain contribution arises at $\Delta n = 0$ from second order processes by non-resonant photon emission/absorption followed by scattering events that ensure conservation of momentum. Whereas stimulated emission is predicted for $\hbar\omega < \epsilon$ (*cf.* Inset: path of stimulated emission), absorption dominates for $\hbar\omega > \epsilon$. A constant in-plane relaxation time of $\tau = 0.2\text{ps}$ is used. Parameters of the GaAs/AlAs-superlattice²⁰: $\Delta = 20.3\text{meV}$, $d = 5.1\text{nm}$, $n^{(2)} = 10^{10}\text{cm}^{-2}$.

We compare the Bloch gain derived within the present approach with the results obtained from the standard model based on semi-classical calculations. In the semi-classical approach³ the Boltzmann equation is solved in the relaxation time approximation for the distribution function $f(k_z, k_{\parallel})$ of miniband electrons subject to an external dc and ac field $F(t) = F + F_{\omega} \cos(\omega t)$, where $F_{\omega} \ll F$. In the case of a Maxwell distribution⁴ this yields

$$\alpha_{sc}(\omega) = \frac{e^2 d^2}{\epsilon_0 n_r c} \frac{\Delta}{2\hbar^2} n^{(3)} \frac{I_1(\Delta/2k_B T)}{I_0(\Delta/2k_B T)} \times \frac{\tau}{1 + (\omega_b \tau)^2} \Re \left(\frac{1 - i\omega\tau - (\omega_b \tau)^2}{(\omega_b \tau)^2 + (1 - i\omega\tau)^2} \right), \quad (25)$$

in the single relaxation time approximation and

$$\alpha_{sc}(\omega) = \frac{e^2 d^2}{\epsilon_0 n_r c} \frac{\Delta}{2\hbar^2} n^{(3)} \frac{I_1(\Delta/2k_B T)}{I_0(\Delta/2k_B T)} \times \frac{\tau_p}{1 + \omega_b^2 \tau_e \tau_p} \Re \left(\frac{1 - i\omega\tau_e - \omega_b^2 \tau_e \tau_p}{\omega_b^2 \tau_e \tau_p + (1 - i\omega\tau_e)(1 - i\omega\tau_p)} \right), \quad (26)$$

for the improved two relaxation time approximation given by Ignatov *et al.*, where distinct momentum and

energy relaxation times τ_p , τ_e are used and which agrees with detailed Monte-Carlo studies²¹. The ratio of Bessel functions contains the temperature dependence for a non-degenerate electron gas. Fig. 4 shows a comparison

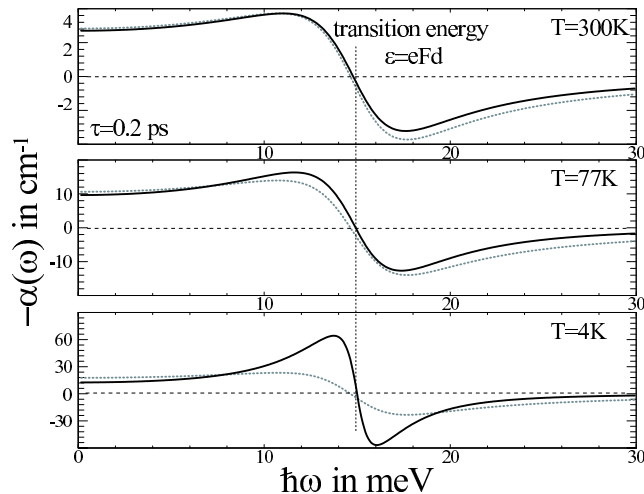


FIG. 4: Semi-classical (dotted line) vs quantum-mechanical results (full line) for the absorption in a superlattice for different temperatures T . We assume a temperature-independent scattering time $\tau = 0.2$ ps in the quantum-mechanical model and set $\tau_{k,e} = \tau$ in the semi-classical model. In the semi-classical picture the peak gain scales with the ratio $I_1(\Delta/2k_B T)/I_0(\Delta/2k_B T)$. The quantum mechanical gain profile exhibits an additional narrowing with lower temperature.

of the semi-classical results and the quantum mechanical predictions for the same constant relaxation time, $\tau = \hbar/\gamma = 0.2$ ps, at different temperatures T . No independent parameters are used. The two approaches agree remarkably well at high temperatures in the semi-classical limit $eFd < \Delta$. The narrowing of the Bloch gain profile with lower temperature, compared to the semi-classical curve, reflects an explicit influence of the electron distribution within the subband. This influence is absent in the semi-classical treatment, regardless of the approximation for the distribution function. In real devices, however, the electron temperature reaches 100 K and above, if the superlattice is biased beyond the onset of Bloch oscillations, according to a self-consistent theoretical analysis of the in-plane distribution function in the Wannier-Stark picture²⁰. Still, at electron temperatures of about 77 K, the considered superlattice, *e.g.*, with a sheet density of $n^{(2)} = 10^{10} \text{ cm}^{-2}$ exhibits a peak material gain of about 15 cm^{-1} , which exceeds the estimated value for waveguide losses in the terahertz range⁸.

B. Quantum cascade laser

In the quantum cascade laser, the populations of the respective subband state depend on the design as well as current and temperature. Then, the inversion gain and a

Bloch type contribution add up as shown in Fig. 5. For a negligible lower state population, $\Delta n/n \approx 1$, where $n = \sum_k (f_k^{22} + f_k^{11})$, equation (20) is dominated by resonant photon emission due to the population inversion between equivalent k -states. It resembles the Lorentzian shaped inversion gain profile, linearly depending on the population inversion Δn . On the other hand, in the limit-

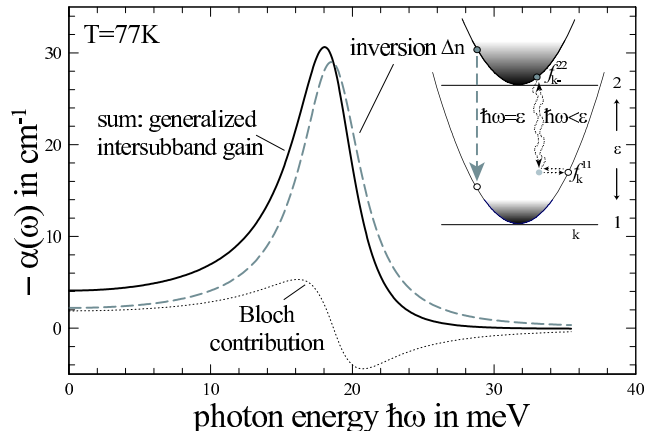


FIG. 5: The population inversion, Δn , leads to nearly symmetric gain profile centered at $\hbar\omega = \epsilon$ (*cf.* left hand side of Inset, dashed line). In addition, the dispersive Bloch gain contributes also here (*cf.* right hand side of Inset, dotted line). The generalized intersubband gain consists of both contributions. Its spectral shape becomes more and more asymmetric with decreasing population inversion. The sample parameters correspond to the terahertz quantum cascade lasers^{7,8} at about $\hbar\omega = 18.7$ meV. A constant relaxation time $\tau = 0.5$ ps and populations $n_2 = 3 \cdot 10^9 \text{ cm}^{-2}$, $n_1 = 1 \cdot 10^9 \text{ cm}^{-2}$ are used, $\Delta n/n \approx 0.5$.

ing case of equal populations, the Bloch type contribution results in a dispersive gain profile as in the superlattice. In between, there is a smooth transition of the (usual) intersubband gain profile to the dispersive Bloch gain with decreasing $\Delta n/n$ as shown in Fig. 6.

Thus, equation (20) for the gain profile states, that *there is a dispersive contribution to the gain profile in any intersubband transition*, with a rising significance for $\Delta n/n$ tending to zero. This result implies two predictions for an intersubband emitter such as the quantum cascade laser. First, the gain does not linearly depend on Δn , but there is a non-negligible intersubband gain even without a population inversion, scaling approximately linearly with the electron density n in the system. Secondly, above threshold, the peak gain and, thus, the laser signal is expected to shift to lower energies with increasing current or temperature, as the ratio $\Delta n/n$ generally decreases.

IV. DISCUSSION

In sections II and III of this paper, the homogeneous broadening γ_k^i of intrasubband relaxation processes has

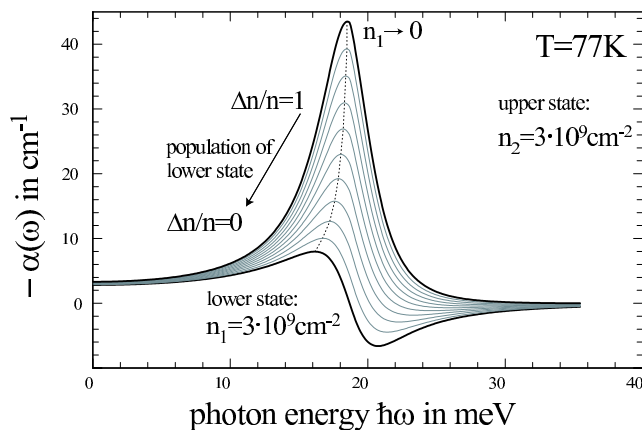


FIG. 6: Evolution of the generalized gain profile from the inversion gain - linearly depending on the population inversion - to the red-shifted Bloch gain with decreasing $\Delta n/n$, respectively increasing the lower state population n_1 , while keeping the upper state density n_2 constant.

been introduced, without specifying it in detail. For the numerical evaluations it was taken as k -independent quantity. As mentioned before, a realistic calculation for microscopic interaction processes in a superlattice will be given elsewhere¹⁹. Moreover, the effect of inhomogeneous level broadening due to interface roughness has not yet been discussed. Inhomogeneity can be considered in a simplified approach such as the "local quantum-mechanical model"^{22,23}. This model assumes a "global quasi-Fermi-level" in each subband, independent of the in-plane position. Within this model the dispersive shape of the Bloch gain is not obscured by inhomogeneous broadening. This holds true even in a diagonal structure²⁴, where the subband fluctuations are not correlated, though the line width will be determined by inhomogeneous broadening²⁵. Furthermore, intersubband plasmons are known to alter the line shape of the intersubband transition and to cause a blue-shift of the intersubband resonance due to dynamical screening of the dipole field²⁶. However, the subband states of a Bloch oscillator or quantum cascade laser are generally weakly populated $\approx 10^{10} \text{cm}^{-2}$ compared to the onset of the collective phenomena²⁷ beyond some 10^{11}cm^{-2} .

In conclusion, the proposed model provides a unified description of optical transitions between two-dimensional subbands. The upper and lower subband

can be either of the same kind (superlattice) or of different kind (quantum cascade laser structure).

In a superlattice a population inversion between equivalent states differing in energy by $\epsilon = eFd$ cannot occur, as $f_k^{22} = f_k^{11}$, due to the translational symmetry of the system. Consequently, resonant stimulated photon emission processes are exactly balanced by the corresponding absorption processes. However, non-resonant second order processes exhibit gain for $\hbar\omega < \epsilon$, whereas net absorption occurs for $\hbar\omega > \epsilon$. This inversionless gain at $\hbar\omega < \epsilon$ represents the quantum mechanical analogue to the Bloch gain predicted by semi-classical models, which had not been described previously. The quantum-mechanical approach agrees remarkably well with the semi-classical results in the high-temperature limit. In contrast to the miniband picture²⁸, it provides an easily conceivable interpretation of the gain mechanism.

In a quantum cascade laser structure, upper and lower state generally exhibit a different population, and in the ideal case, an inverted population. If the inversion decreases, the quasi-symmetric gain spectrum at a high degree of inversion, where $\Delta n/n \approx 1$, evolves to the dispersive Bloch gain, for $\Delta n/n \approx 0$ and below. In contrast to the peak inversion gain, which does not depend on temperature and decreases with scattering, the latter decreases with temperature as the differences in occupation between initial and final states diminish, but increases with more frequent scattering processes.

The theory predicts amplification without inversion below the intersubband resonance of two broadened states. The peak gain in any amplified intersubband transition relying on a poor population inversion, *i.e.* $\Delta n/n \approx 0$, exhibits a red-shift of the order of the level broadening γ with respect to the transition energy. This dispersive gain contribution, that is responsible for the Bloch oscillator effect and which escaped observation so far, is expected to be experimentally accessible in a quantum cascade structure by a search for the attributed red-shift.

Acknowledgements

We would like to thank Andreas Wacker, Daniel Körner and Giacomo Scalari for fruitful discussions. This work was supported by the Swiss National Science Foundation.

* Electronic address: harald.willenberg@unine.ch

¹ L. Esaki and R. Tsu, IBM J. Res. Develop. **14**, 61 (1970).

² R. Kazarinov and R. Suris, Sov. Phys. Semicond. **5**, 707 (1971).

³ S. Ktitorov, G. Simin, and V. Sindalovskii, Fiz. tverd. Tela. **13**, 2230 (1971).

⁴ A. Ignatov and Y. Romanov, Phys. Stat. Sol. B **73**, 327 (1976).

⁵ J. Faist, F. Capasso, D. Sivco, C. Sirtori, A. Hutchinson, and A. Cho, Science **264**, 553 (1994).

⁶ M. Beck, D. Hofstetter, T. Aellen, J. Faist, U. Oesterle, M. Ilegems, E. Gini, and H. Melchior, Science **295**, 301 (2002).

⁷ R. Köhler, A. Tredicucci, F. Beltram, H. Beere, G. Davies, E. Linfield, D. Ritchie, R. C. Iotti, and F. Rossi, Nature **417**, 156 (2002).

- ⁸ M. Rochat, L. Ajili, H. Willenberg, J. Faist, H. Beere, G. Davies, E. Linfield, and D. Ritchie, *App. Phys. Lett.* (2002), unpublished.
- ⁹ A. Sibille, J. Palmier, H. Wang, and F. Mollot, *Phys. Rev. Lett.* **64**, 52 (1990).
- ¹⁰ J. Feldmann, K. Leo, J. Shah, D. Miller, J. Cunningham, T. Meier, G. Plessen, A. Schulze, P. Thomas, and S. Schmitt-Rink, *Phys. Rev. B* **46**, 7252 (1992).
- ¹¹ B. Keay, S. Zeuner, S. Allen, K. Maranowski, A. Gossard, U. Bhattacharya, and M. Rodwell, *Phys. Rev. Lett.* **75**, 4102 (1995).
- ¹² K. Unterrainer, B. Keay, M. Wanke, S. Allen, D. Leonard, U. B. G. Medeiros-Ribeiro, and M. Rodwell, *Phys. Rev. Lett.* **76**, 2973 (1996).
- ¹³ R. Kazarinov and R. Suris, *Sov. Phys. Semicond.* **6**, 120 (1972).
- ¹⁴ W. Kohn, *Phys. Rev.* **15**, 809 (1959).
- ¹⁵ W. Kohn and J. M. Luttinger, *Phys. Rev.* **108**, 590 (1957).
- ¹⁶ A. Wacker, in *Theory of Transport Properties of Semiconductor Nanostructures*, edited by E. Schöll (Chapman and Hall, London, 1998), p. 321.
- ¹⁷ A. Wacker, A.-P. Jauho, S. Zeuner, and S. J. Allen, *Phys. Rev. B* **97**, 13268 (1997).
- ¹⁸ K. Unterrainer, in *Intersubband transitions in quantum wells: Physics and device applications II*, edited by H. Liu and F. Capasso (Academic Press, 2000), vol. 66, chap. 4, p. 139.
- ¹⁹ A. B. Schmidt, H. Willenberg, J. Faist, and G. H. Döhler, unpublished.
- ²⁰ S. Rott, P. Binder, N. Linder, and G. H. Döhler, *Phys. Rev. B* **59**, 7334 (1999).
- ²¹ Provided momentum and energy relaxation times are deduced from microscopic scattering rates, equation (26) is in excellent agreement with Monte-Carlo calculations, whereas the single relaxation time approximation systematically overestimates the semi-classical gain, unpublished results.
- ²² C. Metzner, K. Schrüfer, U. Wieser, M. Luber, M. Kneissl, and G. H. Döhler, *Phys. Rev. B* **51**, 5106 (1995).
- ²³ H. Willenberg, O. Wolst, R. Elpelt, W. Geisselbrecht, S. Malzer, and G. H. Döhler, *Phys. Rev. B* **65**, 35328 (2002).
- ²⁴ Assume $\Delta n = 0$. A pair of subbands with energy separation $\Delta\epsilon_{ij} < \epsilon$ resembles subbands with a population inversion $\Delta n/n > 0$, as the quasi-Fermi-level in the upper subband is higher, regardless of its absolute position, than in the lower state, which follows from $\Delta\epsilon_{ij} < \Phi_i - \Phi_j$. However, subbands spaced by more than the average transition energy, $\Delta\epsilon_{ij} > \epsilon$, contribute with a line shape corresponding to $\Delta n/n < 0$. Hence, inhomogeneous broadening does not average over the dispersive profile.
- ²⁵ K. Campman, H. Schmidt, A. Imamoglu, and A. Gossard, *Appl. Phys. Lett.* **69**, 2554 (1996).
- ²⁶ R. Warburton, C. Gauer, A. Wixforth, J. Kotthaus, B. Brar, and H. Kroemer, *Superlatt. Microstruct.* **19**, 365 (1996).
- ²⁷ S. Luin, V. Pellegrini, F. Beltram, X. Marcadet, and C. Sirtori, *Phys. Rev. B* **64**, 041306 (2001).
- ²⁸ H. Kroemer, *On the nature of the negative-conductivity resonance in a superlattice Bloch oscillator*, cond-mat, 0007482, (2001).

Appendix: Mathematical Details

A. Non-diagonal part $f_{kk'}^{ij}$

Equation (9) governs the dynamics of the non-diagonal part in k, k'

$$\begin{aligned} i\hbar s f_{kk'}^{ij} &\approx i\hbar s \rho_{kk'}^{ij}(0) + \sum_m (V_{kk'}^{im} f_{k'}^{mj} - f_k^{im} V_{kk'}^{mj}) \\ &+ \sum_m (H_k^{im} f_{kk'}^{mj} - f_{kk'}^{im} H_{k'}^{mj}). \end{aligned} \quad (27)$$

Assuming intra-well scattering only, the second and third term on the RHS yield

$$\begin{aligned} \sum_m (V_{kk'}^{im} f_{k'}^{mj} - f_k^{im} V_{kk'}^{mj}) &\approx V_{kk'}^{ii} f_{k'}^{ij} - f_k^{ij} V_{kk'}^{jj} \\ \sum_m (H_k^{im} f_{kk'}^{mj} - f_{kk'}^{im} H_{k'}^{mj}) &= \\ &= (\epsilon_{ik} - \epsilon_{jk'}) f_{kk'}^{ij} + \hbar\Omega_{ij} (f_{kk'}^{jj} - f_{kk'}^{ii}). \end{aligned}$$

Neglecting the non-diagonal matrix element $\rho_{kk'}^{ij}(0)$ and taking the Laplace average equation (27) gives

$$f_{kk'}^{ij} = - \left(\mathcal{P} \frac{1}{\epsilon_{ik} - \epsilon_{jk'}} - i\pi\delta(\epsilon_{ik} - \epsilon_{jk'}) \right) \quad (28)$$

$$\times \left(\hbar\Omega_{ij} (f_{kk'}^{jj} - f_{kk'}^{ii}) + V_{kk'}^{ii} f_{k'}^{ij} - f_k^{ij} V_{kk'}^{jj} \right).$$

The non-diagonal $f_{kk'}^{ij}$ still depends on $f_{kk'}^{jj} - f_{kk'}^{ii}$. The coherences between states k and k' within the same subband are derived from the special version for $i = j$ of equation (27)

$$\begin{aligned} i\hbar s f_{kk'}^{ii} &\approx i\hbar s \rho_{kk'}^{ii}(0) + \sum_m (V_{kk'}^{im} f_{k'}^{mi} - f_k^{im} V_{kk'}^{mi}) \\ &+ \sum_m (H_k^{im} f_{kk'}^{mi} - f_{kk'}^{im} H_{k'}^{mi}), \end{aligned} \quad (29)$$

where the second and third term are evaluated as

$$\begin{aligned} \sum_m (V_{kk'}^{im} f_{k'}^{mi} - f_k^{im} V_{kk'}^{mi}) &= V_{kk'}^{ii} (f_{k'}^{ii} - f_k^{ii}) \\ \sum_m (H_k^{im} f_{kk'}^{mi} - f_{kk'}^{im} H_{k'}^{mi}) &= \\ &= (\epsilon_{ik} - \epsilon_{ik'}) f_{kk'}^{ii} + \hbar\Omega_{ij} f_{kk'}^{jj} - f_{kk'}^{ij} \hbar\Omega_{ji} \\ &\approx (\epsilon_{ik} - \epsilon_{ik'}) f_{kk'}^{ii} \end{aligned}$$

and terms of higher order in the tunneling matrix element corresponding to multiple tunneling processes are neglected. Taking the Laplace average yields

$$f_{kk'}^{ii} = -\mathcal{P} \frac{1}{\epsilon_{ik} - \epsilon_{ik'}} V_{kk'}^{ii} (f_{k'}^{ii} - f_k^{ii}) + \quad (30)$$

$$+i\pi\delta(\epsilon_{ik} - \epsilon_{ik'})V_{kk'}^{ii}(f_{k'}^{ii} - f_k^{ii}) \approx \frac{V_{kk'}^{ii}(f_k^{ii} - f_{k'}^{ii})}{\epsilon_{ik} - \epsilon_{ik'}}.$$

The last term vanishes as either the δ -function or the difference in populations is zero. Placing the approxima-

tions for $f_{kk'}^{ii}$ and $f_{kk'}^{jj}$ in equation (27) and neglecting the principal value yields

$$f_{kk'}^{ij} = i\pi\delta(\epsilon_{ik} - \epsilon_{jk'}) \left(\hbar\Omega_{ij} \left(\frac{V_{kk'}^{jj}(f_k^{jj} - f_{k'}^{jj})}{\epsilon_{jk} - \epsilon_{jk'}} - \frac{V_{kk'}^{ii}(f_k^{ii} - f_{k'}^{ii})}{\epsilon_{ik} - \epsilon_{ik'}} \right) + V_{kk'}^{ii}f_{k'}^{ij} - f_k^{ij}V_{kk'}^{jj} \right). \quad (31)$$

B. Diagonal part f_k^{ij}

Equation (8) determines the dynamics of the diagonal part in k

$$i\hbar s f_k^{ij} = i\hbar s \rho_k^{ij}(0) + \sum_m (H_k^{im} f_k^{mj} - f_k^{im} H_k^{mj}) + \sum_{m,k'} (V_{kk'}^{im} (f)_{k'k}^{mj} - (f)_{kk'}^{im} V_{k'k}^{mj}), \quad (32)$$

where (f) denotes the previous approximations of the non-diagonal part. The second term on the RHS is given by

$$\begin{aligned} \sum_m (H_k^{im} f_k^{mj} - f_k^{im} H_k^{mj}) &= \\ &= (\epsilon_{ik} - \epsilon_{jk}) f_k^{ij} + \hbar\Omega_{ij} (f_k^{jj} - f_k^{ii}) \end{aligned}$$

Performing the Laplace limit $s \rightarrow 0$ we obtain

$$\begin{aligned} (\epsilon_{ik} - \epsilon_{jk}) f_k^{ij} &= \hbar\Omega_{ij} (f_k^{ii} - f_k^{jj}) \\ &- \sum_{k'} (V_{kk'}^{ii} (f)_{k'k}^{ij} - (f)_{kk'}^{ij} V_{k'k}^{jj}) \end{aligned} \quad (33)$$

If one assumes no correlation between scattering events due to the impurities in different wells, *i.e.* were to drop terms containing the product $V_{kk'}^{ii}V_{kk'}^{jj}$ for $i \neq j$, the product of scattering potentials and the approximated non-diagonal part becomes

$$V_{kk'}^{ii} (f)_{k'k}^{ij} = i\pi\delta(\epsilon_{ik'} - \epsilon_{jk}) |V_{kk'}^{ii}|^2 \times \left(f_k^{ij} + \frac{\hbar\Omega_{ij}(f_k^{ii} - f_k^{jj})}{\epsilon_{ik'} - \epsilon_{ik}} \right)$$

and similarly

$$(f)_{kk'}^{ij} V_{k'k}^{jj} = i\pi\delta(\epsilon_{ik} - \epsilon_{jk'}) |V_{kk'}^{jj}|^2 \times \left(f_k^{ij} + \frac{\hbar\Omega_{ij}(f_k^{jj} - f_k^{ii})}{\epsilon_{jk} - \epsilon_{jk'}} \right)$$

Rewriting equation (34) and sorting terms finally leads to an equation for the relevant coherences between the two states, that determine transport properties such as the current density

$$\begin{aligned} (\epsilon_{ik} - \epsilon_{jk}) f_k^{ij} - i\pi f_k^{ij} \sum_{k'} \overbrace{\delta(\epsilon_{ik'} - \epsilon_{jk}) |V_{kk'}^{ii}|^2 + \delta(\epsilon_{ik} - \epsilon_{jk'}) |V_{kk'}^{jj}|^2}^{\text{transition broadening}} &= \overbrace{\hbar\Omega_{ij} (f_k^{ii} - f_k^{jj})}^{\text{population inversion} \rightarrow f^{ac}} \\ + i\pi \sum_{k'} \underbrace{\delta(\epsilon_{ik'} - \epsilon_{jk}) |V_{kk'}^{ii}|^2 \frac{\hbar\Omega_{ij}}{\epsilon_{ik'} - \epsilon_{ik}} (f_k^{ii} - f_k^{jj}) + \delta(\epsilon_{ik} - \epsilon_{jk'}) |V_{kk'}^{jj}|^2 \frac{\hbar\Omega_{ij}}{\epsilon_{jk} - \epsilon_{jk'}} (f_k^{jj} - f_k^{ii})}_{\text{Bloch type contribution} \rightarrow f^{bo}} &. \end{aligned} \quad (34)$$

It corresponds to the results of Kazarinov and Suris¹³ after performing a non-correlated ensemble average on their equation and specifying on a two-level system.

C. Absorption

The ac-field induced coherence is given by the transformation

$$\delta f_{k,\omega}^{21} = -\frac{e d f_\omega}{\hbar \omega} f_{k,\epsilon - \hbar \omega}^{21}, \quad (35)$$

which yields

$$\delta f_k^{21} = -\frac{edf_\omega}{\hbar\omega} \left\{ \frac{\hbar\Omega_{21}(f_k^{22} - f_k^{11})}{\epsilon - \hbar\omega - i(\gamma_k^2 + \gamma_k^1)} + \frac{i\hbar\Omega_{21}(\gamma_k^2(f_{k-}^{22} - f_k^{22}) - \gamma_k^1(f_{k+}^{11} - f_k^{11}))}{(\epsilon - \hbar\omega)(\epsilon - \hbar\omega - i(\gamma_k^2 + \gamma_k^1))} \right\}.$$

As each $\delta f = \delta(f^{qc} + f^{bo})$ the absorption consists of two contributions

$$\alpha(\omega) = \alpha^{qc}(\omega) + \alpha^{bo}(\omega), \quad (36)$$

like the two contributions on the RHS of equation (34) add up in respect to the current density. We obtain

$$\alpha^{qc}(\omega) = \frac{e^2 d^2 |\Omega_{21}|^2}{\varepsilon_0 n_r c \omega} \sum_k \left(\frac{\hbar\tau_k^{-1}}{(\epsilon + \hbar\omega)^2 + (\hbar\tau_k^{-1})^2} - \underbrace{\frac{\hbar\tau_k^{-1}}{(\epsilon - \hbar\omega)^2 + (\hbar\tau_k^{-1})^2}}_{\text{main contribution}} \right) (f_k^{22} - f_k^{11}) \quad (37)$$

and

$$\alpha^{bo}(\omega) = \frac{e^2 d^2 |\Omega_{21}|^2}{\varepsilon_0 n_r c \omega} \sum_k \left(\frac{\gamma_k^2(f_{l-}^{22} - f_k^{22}) - \gamma_k^1(f_{l+}^{11} - f_k^{11})}{(\epsilon + \hbar\omega)^2 + (\hbar\tau_k^{-1})^2} - \underbrace{\frac{\gamma_k^2(f_{k-}^{22} - f_k^{22}) - \gamma_k^1(f_{k+}^{11} - f_k^{11})}{(\epsilon - \hbar\omega)^2 + (\hbar\tau_k^{-1})^2}}_{\text{main contribution}} \right), \quad (38)$$

where we set $k_\pm = \hbar^{-1}\sqrt{2m^*(\epsilon_k \pm (\epsilon - \hbar\omega))}$, $l_\pm = \hbar^{-1}\sqrt{2m^*(\epsilon_k \pm (\epsilon + \hbar\omega))}$ and $\hbar\tau_k^{-1} = \gamma_k^1 + \gamma_k^2$. The first term, $\alpha^{qc}(\omega)$, depends on the difference in population of equivalent k -states and yields the usual Lorentzian line shape for the gain profile in case of a population inversion. The second contribution, $\alpha^{bo}(\omega)$, contains differences of populations between different k -states within the respective subband state and will be discussed later.

In the following, we will omit the non-resonant contribution. The contribution accounts for the situation where the upper state lies below the lower state. However, it is not neglected in the numerical calculations as it is important to prevent the divergence at $\omega = 0$, which alters the line-shape for $\hbar\omega \sim \mathcal{O}(\gamma)$, *i.e.* in the far-infrared or terahertz regime. If one regards the resonant contri-

bution only, the inversion gain reads

$$\alpha^{qc}(\omega) = \frac{e^2 d^2 |\Omega_{21}|^2}{\varepsilon_0 n_r c \omega} \sum_k \frac{\hbar\tau_k^{-1}(f_k^{11} - f_k^{22})}{(\epsilon - \hbar\omega)^2 + (\hbar\tau_k^{-1})^2}$$

whereas the Bloch type contribution gives

$$\alpha^{bo}(\omega) = \frac{e^2 d^2 |\Omega_{21}|^2}{\varepsilon_0 n_r c \omega} \sum_k \frac{\gamma_k^1(f_{k+}^{11} - f_k^{11}) - \gamma_k^2(f_{k-}^{22} - f_k^{22})}{(\epsilon - \hbar\omega)^2 + (\hbar\tau_k^{-1})^2}.$$

The difficulty in assigning a path of transitions of the electron to the latter expression for $\alpha^{bo}(\omega)$ is resolved by adding both contributions (*cf.* equation (19)).